



This is a repository copy of *Moment method analysis of an archimedean spiral printed on a layered dielectric sphere*.

White Rose Research Online URL for this paper:
<http://eprints.whiterose.ac.uk/9824/>

Article:

Khamas, S.K. (2008) Moment method analysis of an archimedean spiral printed on a layered dielectric sphere. *IEEE Transactions on Antennas and Propagation*, 56 (2). pp. 345-352. ISSN 0018-926X

<https://doi.org/10.1109/TAP.2007.915466>

Reuse

Unless indicated otherwise, fulltext items are protected by copyright with all rights reserved. The copyright exception in section 29 of the Copyright, Designs and Patents Act 1988 allows the making of a single copy solely for the purpose of non-commercial research or private study within the limits of fair dealing. The publisher or other rights-holder may allow further reproduction and re-use of this version - refer to the White Rose Research Online record for this item. Where records identify the publisher as the copyright holder, users can verify any specific terms of use on the publisher's website.

Takedown

If you consider content in White Rose Research Online to be in breach of UK law, please notify us by emailing eprints@whiterose.ac.uk including the URL of the record and the reason for the withdrawal request.



eprints@whiterose.ac.uk
<https://eprints.whiterose.ac.uk/>

Moment Method Analysis of an Archimedean Spiral Printed on a Layered Dielectric Sphere

Salam K. Khamas, *Member, IEEE*

Abstract—A method of moments model is presented to analyze Archimedean spirals that are printed on a layered dielectric sphere. The model is derived assuming an arbitrary location of the spiral. Input impedance, current distribution and far-field results are presented and are shown to be in good agreements with other methods.

Index Terms—Method of moments (MoM), spherical antennas, spiral antennas.

I. INTRODUCTION

OVER THE LAST two decades spiral antennas have received increased interest due to their wide bandwidths, high efficiencies and circular polarization. Spiral antennas in different shapes and configurations have been considered in the literature. An Archimedean spiral radiating above a perfectly conducting ground plane has been reported in [1]. A curl antenna, which is a single arm spiral fed by a monopole has been presented in [2]. Eccentric spirals that offer advantages of beam steering have been reported in [3], [4]. Moment method and FDTD have been used to model spirals printed on layered dielectric substrates [5]–[7]. Most of these analysis and measurements have been limited to planar geometries.

A conformal spiral has been reported in [8], [9], where a single square spiral and an array of square spirals above and in conformance with a perfectly conducting cylindrical ground plane have been modelled and measured. A spherical array of spirals has been reported in [10], the array elements are planar Archimedean spirals placed around an imaginary spherical surface to provide full-scan coverage.

Archimedean spirals that conform to a spherical surface or that are printed on a layered dielectric sphere have not been considered earlier. This study presents analysis of such antennas using the method of moments (MoM) where the dyadic Green's functions have been used to model the effects of the sphere [11]–[15]. Two configurations have been considered including a conformal Archimedean spiral above a perfectly conducting sphere and a spiral printed on a grounded spherical substrate. For each spiral the input impedance, radiation pattern, gain and axial ratio are presented. These results have been compared with controls calculated using CST microwave studio [16]. The input impedance of a spiral radiating next to a large sphere has been

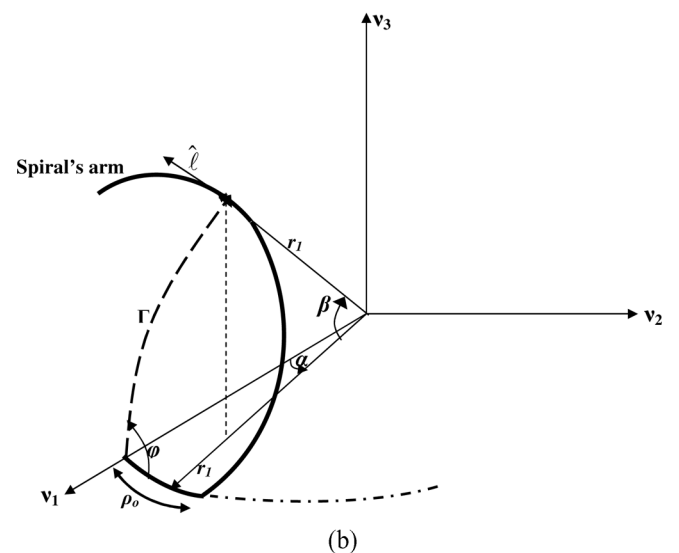
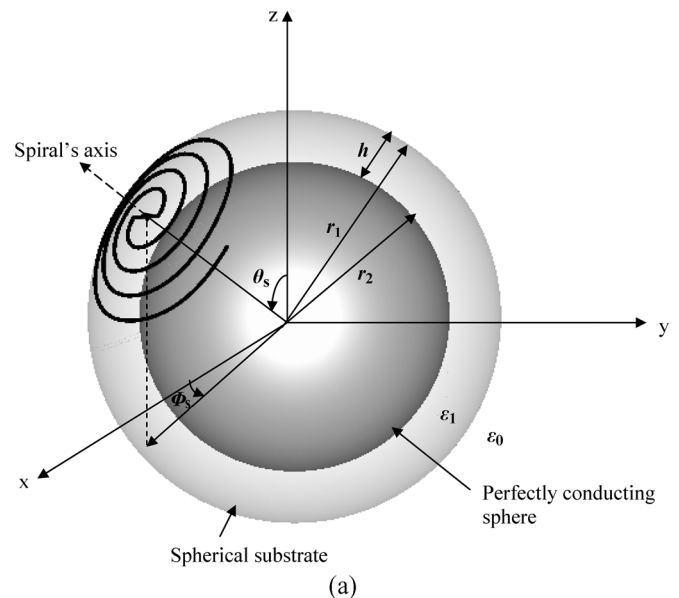


Fig. 1. (a) Archimedean spiral printed on a layered dielectric sphere. (b) Local angles α , β and the spiral winding angle φ .

calculated and compared with that of an equivalent planar spiral above a flat substrate [1], [17].

II. THEORY AND FORMULATION

A. Spiral's Geometry

Fig. 1(a) shows a conformal Archimedean spiral in a three-layer media: the first layer is free space, the second is a spherical

Manuscript received May 4, 2007; revised August 30, 2007.

The author is with the Department of Electronic and Electrical Engineering, University of Sheffield, Sheffield S1 3JD, U.K. (email: s.khamas@sheffield.ac.uk).

Digital Object Identifier 10.1109/TAP.2007.915466

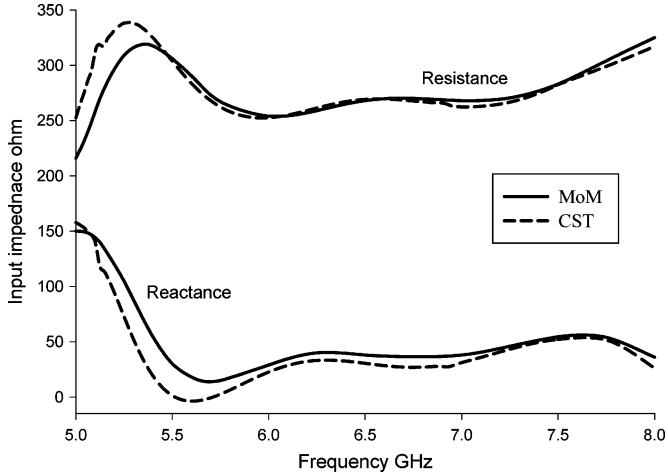


Fig. 2. Input impedance of a spiral above a 1.5 cm perfectly conducting sphere.

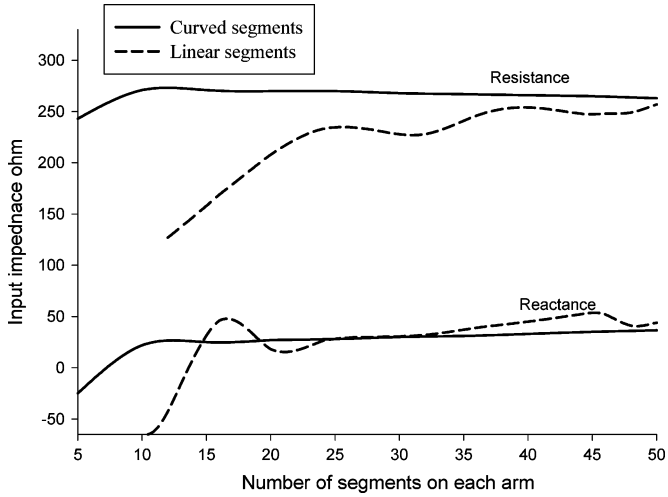


Fig. 3. Convergence of input impedance of a spiral above a 1.5 cm perfectly conducting sphere at 6.5 GHz.

substrate and the third layer is a perfectly conducting sphere. The spherical substrate has a dielectric constant of ϵ_1 and a thickness of h , the perfectly conducting sphere has radius of r_2 and the overall radius of the layered sphere is r_1 . The spiral's center is positioned at (r_1, θ_s, Φ_s) .

To define the spiral arm the local angles β and α , which are shown in Fig. 1(b), have been defined as

$$\beta = \frac{\Gamma \sin \varphi}{r_1} \quad (1)$$

$$\alpha = \frac{\Gamma \cos \varphi}{r_1 \cos \beta} \quad (2)$$

where $\Gamma = \rho_o + a\varphi$, a is the spiral constant, ρ_o is the length of the feed segment and φ is the winding angle of the spiral. The local co-ordinates are

$$\nu_1 = r_1 \cos \beta \cos \alpha \quad (3)$$

$$\nu_2 = r_1 \cos \beta \sin \alpha \quad (4)$$

$$\nu_3 = r_1 \sin \beta. \quad (5)$$

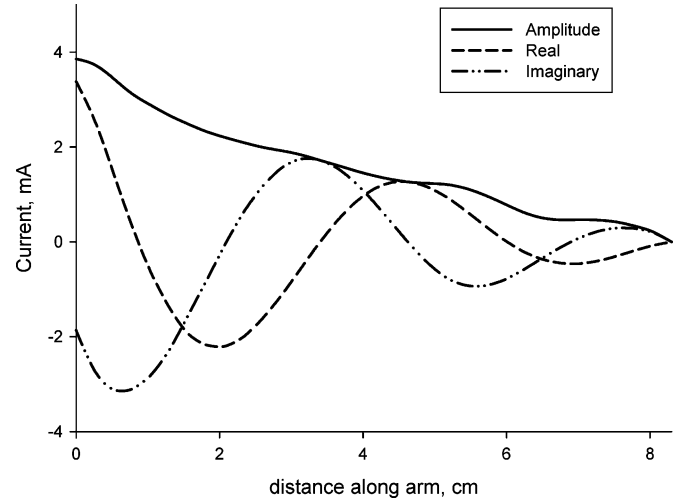


Fig. 4. Current's distribution along one arm of a spiral above a perfectly conducting sphere at 6.5 GHz.

By using vectors rotation [18], the required equations to define a spiral arm can then be derived as

$$x = \cos \phi_s (\nu_1 \sin \theta_s - \nu_3 \cos \theta_s) - \nu_2 \sin \phi_s \quad (6)$$

$$y = \sin \phi_s (\nu_1 \sin \theta_s - \nu_3 \cos \theta_s) + \nu_2 \cos \phi_s \quad (7)$$

$$z = \nu_1 \cos \theta_s + \nu_3 \sin \theta_s. \quad (8)$$

A unit tangent vector to the spiral arm can be obtained as [18]

$$\hat{l} = \frac{1}{\sqrt{\left(\frac{dx}{d\varphi}\right)^2 + \left(\frac{dy}{d\varphi}\right)^2 + \left(\frac{dz}{d\varphi}\right)^2}} \left(\frac{dx}{d\varphi} \hat{x} + \frac{dy}{d\varphi} \hat{y} + \frac{dz}{d\varphi} \hat{z} \right). \quad (9)$$

Equation (9) can be expressed in a more convenient form as

$$\hat{l} = \ell_\theta \hat{\theta} + \ell_\phi \hat{\phi} \quad (10)$$

where

$$\ell_\theta = \frac{1}{\sqrt{\alpha_d^2 + \beta_d^2}} \times [-\beta_d [\cos \theta \{ \Delta \cos(\phi - \phi_s) + \sin \beta \sin \alpha \sin(\phi - \phi_s) \} + \sin \theta \{ \sin \beta \cos \alpha \cos \theta_s + \cos \beta \sin \theta_s \} + \alpha_d [\cos \theta \{ \cos \alpha \sin(\phi - \phi_s) - \sin \alpha \sin \theta_s \cos(\phi - \phi_s) \} + \sin \theta \sin \alpha \cos \theta_s]] \quad (11)$$

$$\ell_\phi = \frac{1}{\sqrt{\alpha_d^2 + \beta_d^2}} \times [\beta_d [\Delta \sin(\phi - \phi_s) - \sin \beta \sin \alpha \cos(\phi - \phi_s)] + \alpha_d [\cos \alpha \cos(\phi - \phi_s) + \sin \alpha \sin \theta_s \sin(\phi - \phi_s)]] \quad (12)$$

$$\Delta = \sin \beta \cos \alpha \sin \theta_s + \cos \beta \cos \theta_s \quad (13)$$

$$\beta_d = a \sin \varphi + (\rho_o + a\varphi) \cos \varphi \quad (14)$$

$$\alpha_d = (a \cos \varphi - (\rho_o + a\varphi) \sin \varphi) + \alpha \beta_d \sin \beta. \quad (15)$$

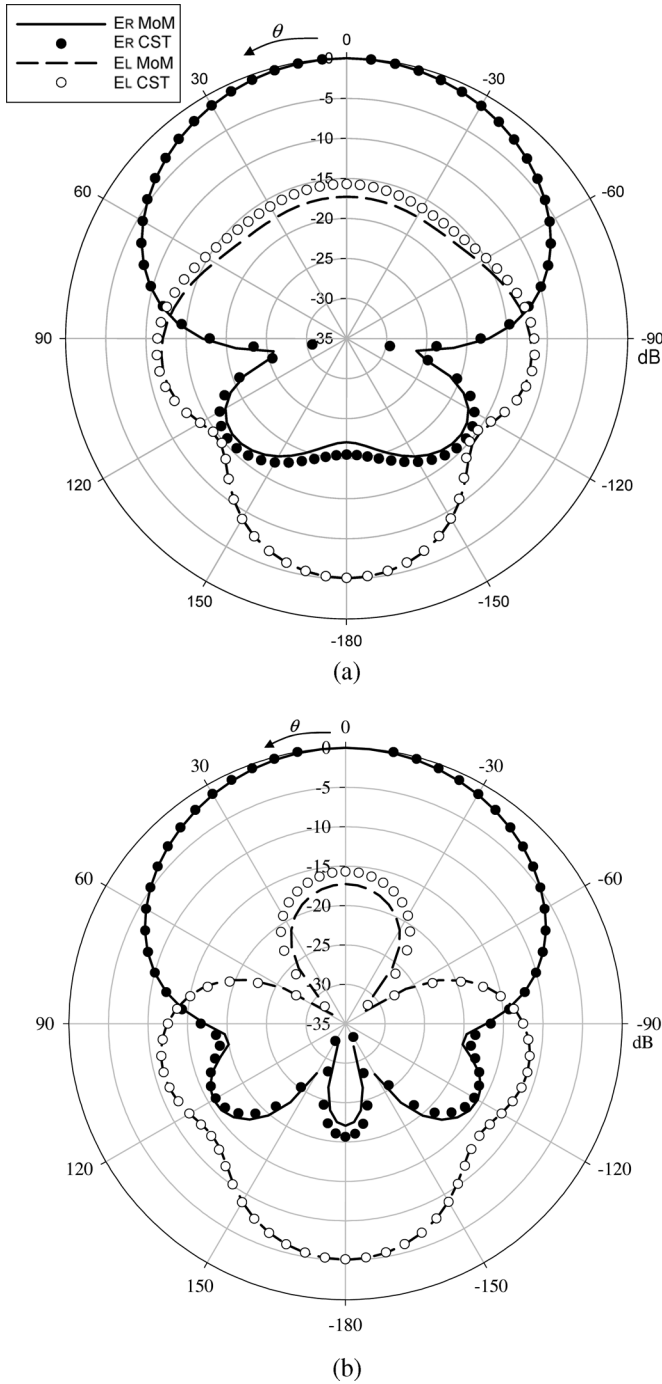


Fig. 5. Radiation pattern of a spiral antenna above a PEC sphere as a function of θ at 6.5 GHz (a) $\phi = 0^\circ$ plane, (b) $\phi = 90^\circ$ plane.

The length of a single spiral arm is given by

$$\ell = \int_0^{\varphi_{\max}} \sqrt{\alpha_d^2 + \beta_d^2} d\varphi. \quad (16)$$

An alternative method to formulate the problem is to assume that the spiral's center is located on the z -axis and then use Eulerian angles to define the spiral's co-ordinates anywhere on the sphere [19].

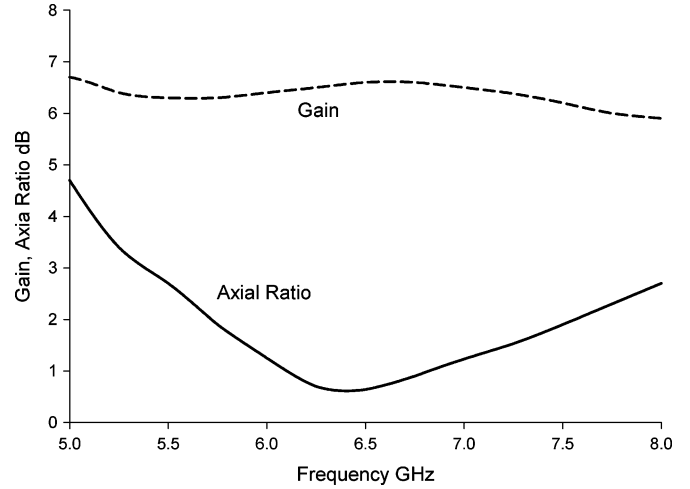


Fig. 6. Axial ratio and gain of a spiral above a perfectly conducting sphere.

B. MoM Solution

By assuming the wire radius to be very small compared to the wavelength, the thin wire approximation can be used. Since there is no radial current component, the remaining current components due to a current with amplitude I_ℓ are

$$I_i = I_\ell \hat{i} \quad (17)$$

where $i = \theta$ or ϕ .

Each spiral arm has been divided into curved segments of length $\Delta\ell$ and curved sinusoidal current testing and expansion functions have been chosen as

$$I_\ell = I_m \frac{\sin(k_o(\Delta\ell - |\ell - \ell_m|))}{\sin(k_o\Delta\ell)} \quad (18)$$

$$I_{\ell'} = I_q \frac{\sin(k_o(\Delta\ell' - |\ell' - \ell_q|))}{\sin(k_o\Delta\ell)} \quad (19)$$

where the primes in (19) denote source co-ordinates.

Dyadic Green's functions (DGF) have been used in the moment method analysis of a spiral radiating in the presence of a sphere. Complete set of expressions of the dyadic Green's functions are given in [13] in form of an infinite summation of spherical waves. When both the source and the field points are in free space, the DGF is [13]

$$\overline{\mathbf{G}}_e^{(11)}(\mathbf{r}, \mathbf{r}') = \overline{\mathbf{G}}_{0e}(\mathbf{r}, \mathbf{r}') + \overline{\mathbf{G}}_{es}^{(11)}(\mathbf{r}, \mathbf{r}') \quad (20)$$

and the corresponding electric field of a thin wire is

$$\mathbf{E} = j\omega\mu_o \int_{\ell'} \left(\overline{\mathbf{G}}_{0e}(\mathbf{r}, \mathbf{r}') + \overline{\mathbf{G}}_{es}^{(11)}(\mathbf{r}, \mathbf{r}') \right) \bullet \mathbf{I}_{\ell'} d\ell' \quad (21)$$

where \mathbf{r} and \mathbf{r}' refer to the location of field and source points respectively.

The first term in (20) and (21), $\overline{\mathbf{G}}_{0e}(\mathbf{r}, \mathbf{r}')$, represents the contribution from a source radiating in an unbounded homogenous

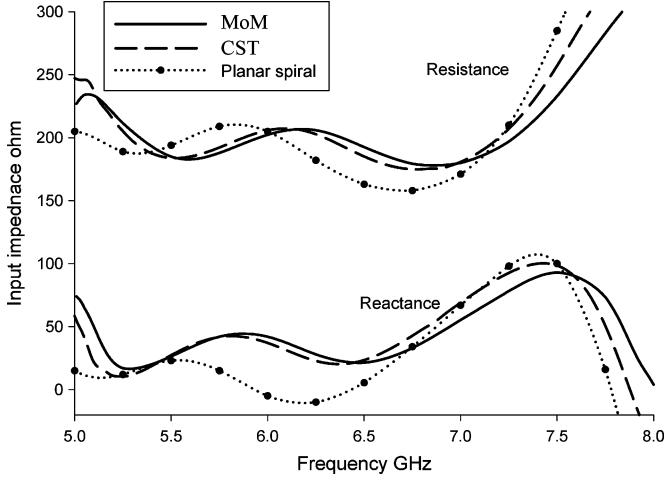


Fig. 7. Input impedance of a spiral printed on a 3 cm layered sphere.

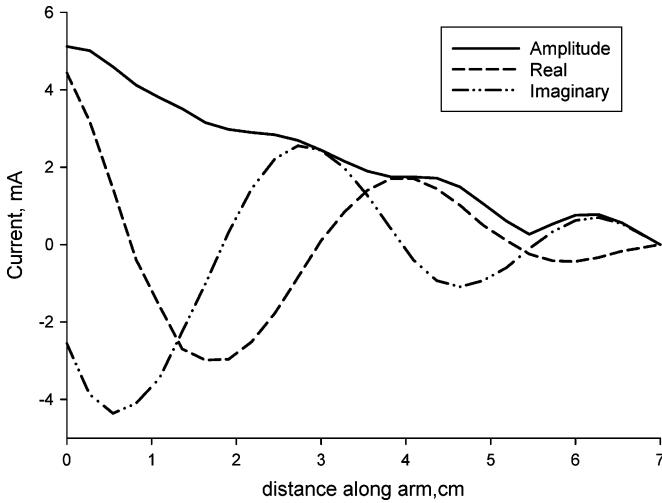


Fig. 8. Current's distribution along one arm of a spiral printed on a 3 cm layered sphere at 6 GHz.

free space, and the second term represents the source contribution due to the presence of the sphere. When the source and field points are very close to each other $\bar{\mathbf{G}}_{0e}(\mathbf{r}, \mathbf{r}')$ converges very slowly, therefore the physical argument technique has been used to express it using the much simpler free space Green's function [20]. Then the tangential field due to the q th expansion current pulse becomes

$$E_{\ell} = j\omega\mu_0 \int_{\ell_{q-1}}^{\ell_{q+1}} \left[I_{\ell'} \left\{ \hat{\ell} \cdot \hat{\ell}' + \frac{\partial^2}{k_0^2 \partial \ell \partial \ell'} \right\} \frac{e^{-jk_0 R}}{4\pi R} + E_{es} \right] d\ell' \quad (22)$$

where $R = \sqrt{(x-x')^2 + (y-y')^2 + (z-z')^2}$, E_{es} is the field component due to the dyadic Green's function $\bar{\mathbf{G}}_{es}^{(11)}(\mathbf{r}, \mathbf{r}')$ which can be expressed as

$$E_{es} = E_{\theta} \ell_{\theta} + E_{\phi} \ell_{\phi} \quad (23)$$

and

$$\begin{bmatrix} E_{\theta} \\ E_{\phi} \end{bmatrix} = \begin{bmatrix} G_{\theta\theta} & G_{\theta\phi} \\ G_{\phi\theta} & G_{\phi\phi} \end{bmatrix} \begin{bmatrix} I_{\theta'} \\ I_{\phi'} \end{bmatrix}. \quad (24)$$

The DGF components in (24) are given by

$$G_{\theta\theta} = \frac{-jk_0}{4\pi} \sum_{n=1}^{\infty} \frac{2n+1}{n(n+1)} (a_n \Delta_1 \zeta_1 + b_n \Delta_2 \zeta_2) \quad (25)$$

$$G_{\theta\phi} = -\sin(\phi - \phi') \frac{jk_0}{4\pi} \times \sum_{n=1}^{\infty} \frac{2n+1}{n(n+1)} (a_n \Delta_3 \zeta_1 + b_n \Delta_4 \zeta_2) \quad (26)$$

$$G_{\phi\theta} = \sin(\phi - \phi') \frac{jk_0}{4\pi} \times \sum_{n=1}^{\infty} \frac{2n+1}{n(n+1)} (a_n \Delta_4 \zeta_1 + b_n \Delta_3 \zeta_2) \quad (27)$$

$$G_{\phi\phi} = \frac{-jk_0}{4\pi} \sum_{n=1}^{\infty} \frac{2n+1}{n(n+1)} (a_n \Delta_2 \zeta_1 + b_n \Delta_1 \zeta_2) \quad (28)$$

where

$$\zeta_1 = h_n^{(2)}(k_0 r) h_n^{(2)}(k_0 r') \quad (29)$$

$$\zeta_2 = \frac{1}{k_0^2 r r'} \frac{\partial}{\partial r} [r h_n^{(2)}(k_0 r)] \frac{\partial}{\partial r'} [r' h_n^{(2)}(k_0 r')] \quad (30)$$

$$\Delta_1 = \left[-\sin^2(\phi - \phi') \sin \theta \sin \theta' \frac{P_n^2(\cos \gamma)}{(\sin \gamma)^2} + \cos(\phi - \phi') \frac{\partial P_n(\cos \gamma)}{\partial(\cos \gamma)} \right] \quad (31)$$

$$\Delta_2 = \left[\frac{\partial \cos \gamma}{\partial \theta} \frac{\partial \cos \gamma}{\partial \theta'} \frac{P_n^2(\cos \gamma)}{(\sin \gamma)^2} + \frac{\partial^2 \cos \gamma}{\partial \theta \partial \theta'} \frac{\partial P_n(\cos \gamma)}{\partial(\cos \gamma)} \right] \quad (32)$$

$$\Delta_3 = \left[\sin \theta' \frac{\partial \cos \gamma}{\partial \theta'} \frac{P_n^2(\cos \gamma)}{(\sin \gamma)^2} + \cos \theta' \frac{\partial P_n(\cos \gamma)}{\partial(\cos \gamma)} \right] \quad (33)$$

$$\Delta_4 = \left[\sin \theta \frac{\partial \cos \gamma}{\partial \theta} \frac{P_n^2(\cos \gamma)}{(\sin \gamma)^2} + \cos \theta \frac{\partial P_n(\cos \gamma)}{\partial(\cos \gamma)} \right] \quad (34)$$

$$\cos \gamma = \cos \theta \cos \theta' + \sin \theta \sin \theta' \cos(\phi - \phi').$$

$h_n^{(2)}(k_0 r)$ is the spherical Hankel function of the second type, $P_n(\cos \gamma)$ is the Legendre function of degree n and $P_n^2(\cos \gamma)$ is the associated Legendre function of the first kind with the order 2 and degree n . Detailed expressions for a_n and b_n are given in [13].

Finally the impedance matrix elements can then be calculated as

$$Z_{mq} = \int_{\ell_{m-1}}^{\ell_{m+1}} \frac{\sin(k_0(\Delta\ell - |\ell - \ell_m|))}{\sin(k_0 \Delta\ell)} \frac{E_{\ell}}{I_q} d\ell. \quad (35)$$

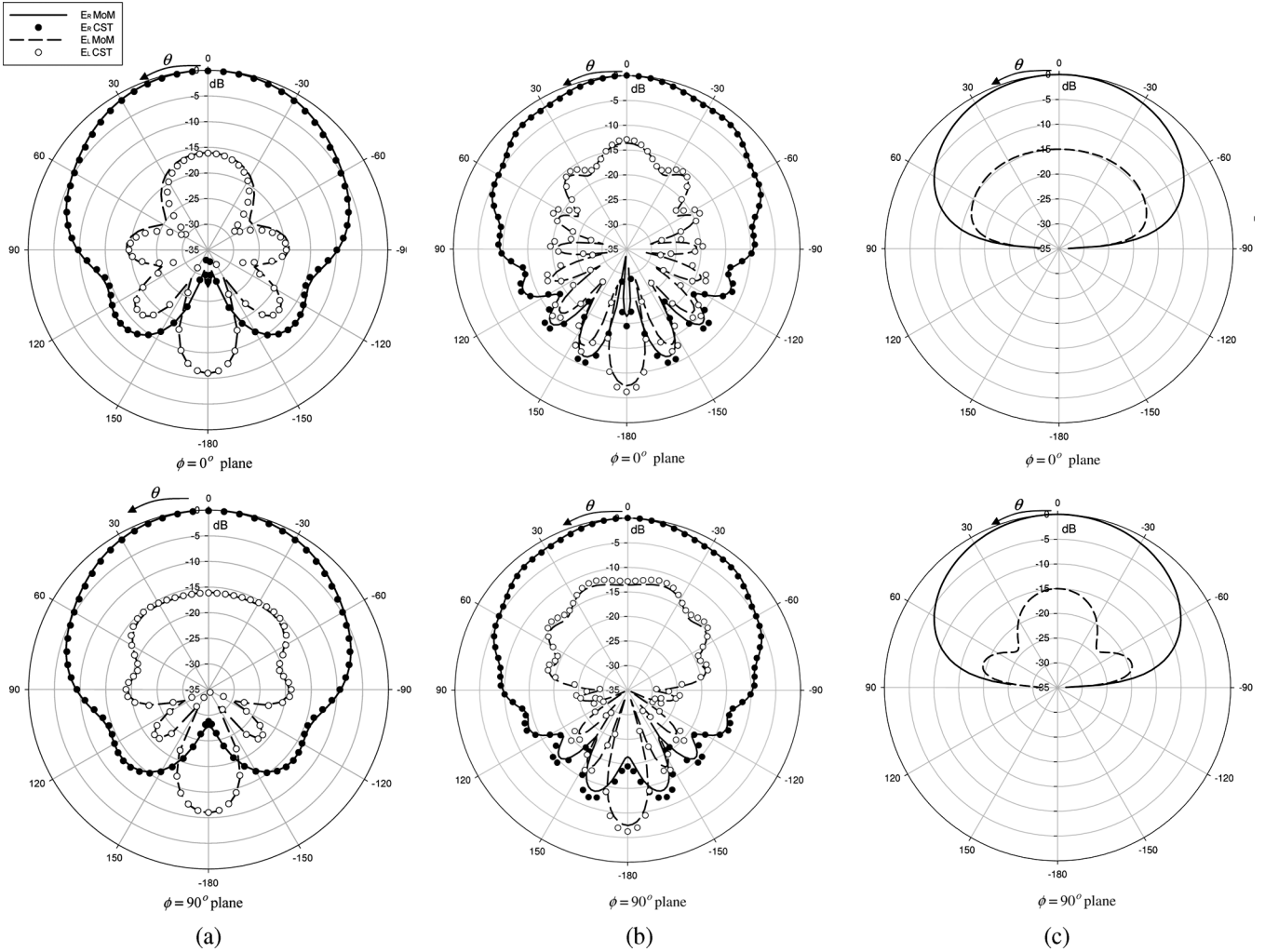


Fig. 9. Radiation pattern of a printed spiral as a function of θ when $h = 0.75$ cm at 6 GHz (a) $r_1 = 3$ cm, (b) $r_1 = 6$ cm, (c) planar spiral.

C. Far-Zone Radiation Fields

Once the current distribution is determined, the far-field components can be derived using the Hankel function asymptotic expressions when $r \rightarrow \infty$, that is

$$h_n^{(2)}(k_0 r) = j^{n+1} \frac{e^{-jk_0 r}}{k_0 r}$$

$$\frac{\partial (r h_n^{(2)}(k_0 r))}{\partial r} = j^n e^{-jk_0 r}.$$

This results are in the following:

$$E_\theta = 30k_0 \frac{e^{-jk_0 r}}{r} \int_{\ell'}^{\infty} \sum_{n=1}^{\infty} \frac{2n+1}{n(n+1)} j^n$$

$$\times \left[j \left(j_n(k_0 r') + a_n h_n^{(2)}(k_0 r') \right) \right.$$

$$\times (\Delta_1 \ell_{\phi'} + \Delta_3 \sin(\phi - \phi') \ell_{\theta'})$$

$$\left. + \frac{\partial \left\{ r' \left(j_n(k_0 r') + b_n h_n^{(2)}(k_0 r') \right) \right\}}{k_0 r' \partial r'} \right]$$

$$\times (\Delta_2 \ell_{\theta'} + \Delta_4 \sin(\phi - \phi') \ell_{\phi'}) I_{\ell'} d\ell' \quad (36)$$

$$E_\phi = 30k_0 \frac{e^{-jk_0 r}}{r} \int_{\ell'}^{\infty} \sum_{n=1}^{\infty} \frac{2n+1}{n(n+1)} j^n$$

$$\times \left[j \left(j_n(k_0 r') + a_n h_n^{(2)}(k_0 r') \right) \right.$$

$$\times (\Delta_2 \ell_{\phi'} - \Delta_4 \sin(\phi - \phi') \ell_{\theta'})$$

$$\left. + \frac{\partial \left\{ r' \left(j_n(k_0 r') + b_n h_n^{(2)}(k_0 r') \right) \right\}}{k_0 r' \partial r'} \right]$$

$$\times (\Delta_1 \ell_{\phi'} - \Delta_3 \sin(\phi - \phi') \ell_{\theta'}) I_{\ell'} d\ell' \quad (37)$$

where $j_n(k_0 r)$ is the spherical Bessel function of order n .

D. General Considerations

The equations derived in section II-A can be used to model the spiral's feed segment by modifying the local angles in (1), (2), (14), and (15) to

$$\alpha = \frac{\ell}{r_1} \quad -\rho_o \leq \ell \leq \rho_o \quad (38)$$

$\alpha_d = 1$ and $\beta = \beta_d = 0$. The dyadic Green's functions in [13] have double summation expressions. For computation effi-

ciency this has been reduced to a single summation by using the addition theorem of Legendre polynomials [21]

$$P_n(\cos \gamma) = \sum_{m=0}^n \frac{2}{\delta_m} \frac{(n-m)!}{(n+m)!} \times P_n^m(\cos \theta) P_n^m(\cos \theta') \cos m(\phi - \phi') \quad (39)$$

where δ_m is 2 for $m = 0$ and 1 for $m > 0$.

CST [16] has been used to validate the MoM code. For each spiral the following CST settings have been used; 40 mesh lines per wavelength and mesh line ratio limit of 30. A gap of 0.05 cm was made in the spiral's feed segment to accommodate the discrete excitation port. CST thin wire approximation and an accuracy of -50dB have been chosen in the CST transient solver.

III. RESULTS

Two spiral geometries have been considered; the first is a spiral above a perfectly conducting sphere and the second is a spiral printed on a layered sphere. To ensure convergence of the MoM code, each spiral arm has been divided into 25 curved segments except in the case of a spiral printed on a large dielectric sphere where 130 curved segments have been used owing to the spiral's arm length. In all cases the spiral's axis was located at $(\theta_s = 0, \phi_s = 0)$ and a delta gap source has been used to feed the antenna.

The free space Green's function in (22) is singular when $\mathbf{r} = \mathbf{r}'$. This is a well known problem which can be avoided by employing the thin wire approximation so that the minimum distance between the source and observation points is equal to the wire radius. More accurate solution can be obtained by calculating the exact kernel [20]. In this study, the input impedance has been calculated assuming the source point is located at $r' = r_1$ and the field point at $r = r_1 + w$, where w is the wire radius that has been chosen as 0.02 cm.

The infinite summation in (25)–(28) is convergent and for a spiral printed on a dielectric sphere it has been truncated at $N = 250$, where N depends on the sphere radius, permittivity, number of layers and the separation between source and field points. For the case of a spiral above a perfectly conducting sphere $N = 30$ was sufficient to achieve convergence. In the far field region convergence of (36) and (37) has been achieved using $N = 15$ for all spirals.

A. Spiral Above a PEC Sphere

The spiral in Fig. 1(a) has been modelled when $\epsilon_1 = \epsilon_0$, i.e. the problem is reduced to that of an Archimedean spiral placed at a height h above a perfectly conducting sphere. The following parameters have been used to model this spiral: feed wire length of $\rho_o = 0.2$ cm, a spiral constant of $a = 0.0764$ cm/rad, a maximum winding angle of $\varphi_{\max} = 12.4$ rad [1], a sphere radius of $r_2 = 1.5$ cm and a height of $h = 1$ cm. The spiral's input impedance has been calculated and shown in Fig. 2 as a function of frequency. Comparison with results obtained using CST proves the accuracy of the presented MoM model. Fig. 3 shows

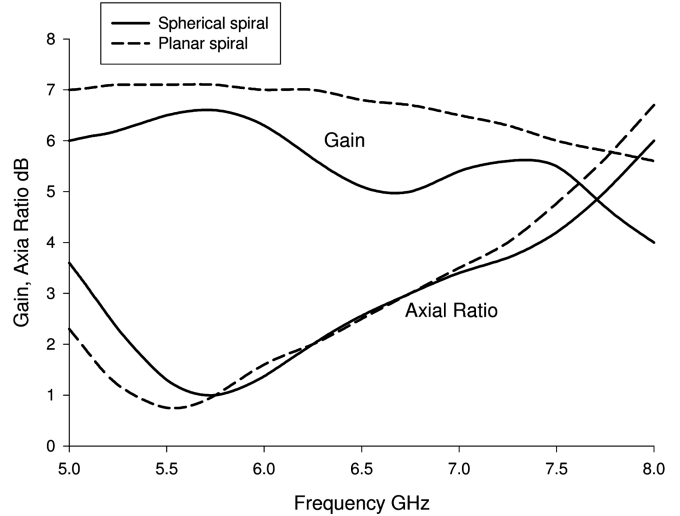


Fig. 10. Axial ratio and gain of a spiral printed on a 3 cm layered dielectric sphere.

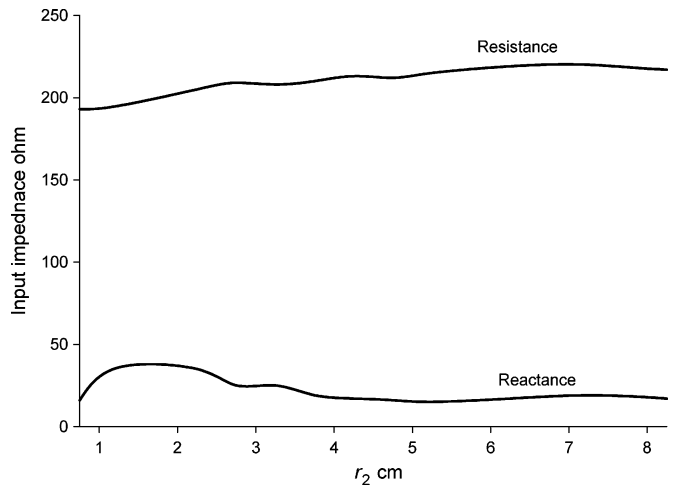


Fig. 11. Input impedance of a printed spherical spiral as a function of r_2 at 6 GHz.

the convergence of input impedance with number of segments when the spiral is modelled using curved and linear segmentation. Curved segmentation approach has improved the convergence rate by a factor of $\kappa > 2$. This should provide reductions on the order of κ in computation time and κ^2 in the required memory space. The linear segmentation results have been obtained using NEC [22]. The current distribution along the spiral arm at 6.5 GHz is shown in Fig. 4 with a predominantly travelling wave distribution. Radiated far fields have been calculated and the right- and left-hand circularly polarized components are shown in Fig. 5 in the $\phi = 0^\circ$ and $\phi = 90^\circ$ planes when compared with those obtained using CST with good agreement. Gain and axial ratio of this spiral are shown in Fig. 6 indicating that the spiral has a gain of 6 dB and an axial ratio 3 dB bandwidth of more than 40%. The same spiral has been modelled in the absence of the PEC sphere at 6.5 GHz and its gain and axial ratio have been calculated as 4.3 dB and 1.9 dB, respectively.

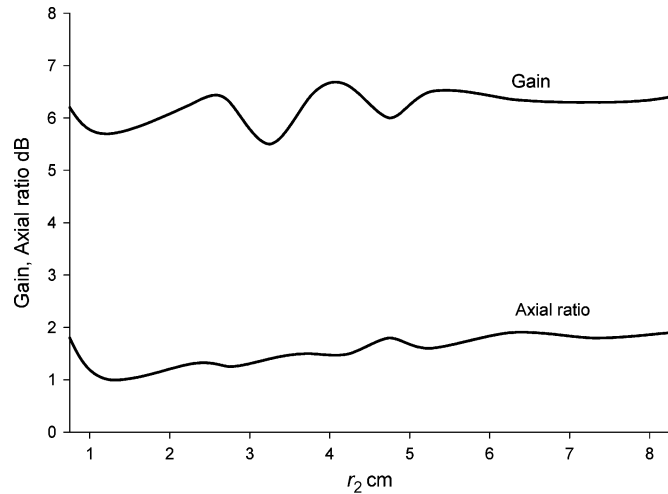


Fig. 12. Axial ratio and gain of a printed spherical spiral as a function of r_2 at 6 GHz.

This shows that the presence of the PEC sphere has improved the spiral's gain and circular polarization.

B. Spiral Printed on a Two-Layer Sphere

The spiral's geometry shown in Fig. 1(a) has been modelled again for the case when the dielectric substrate has a relative permittivity of $\epsilon_{r1} = 2$ and a thickness of $h = 0.75$ cm. The radius of the perfectly conducting sphere has been chosen as $r_2 = 2.25$ cm, so that the layered sphere has an outer radius of $r_1 = 3$ cm. The spiral has been modelled using $\rho_o = 0.163$ cm, a spiral constant of $a = 0.0623$ cm/rad and $\varphi_{\max} = 12.4$ rad. The input impedance has been calculated using MoM and compared with the CST results as shown in Fig. 7. The two sets of results agree well with each other. The input impedance of an equivalent spiral that is printed on an infinite flat substrate has been calculated using a separate MoM code [6] as shown in Fig. 7. A travelling wave current distribution along the spiral arm can be seen in Fig. 8. Far-field components are shown in Fig. 9 for different sphere radii in the $\phi = 0^\circ$ and $\phi = 90^\circ$ planes, where it can be seen that back-lobes exist because of the finite size perfectly conducting spherical core. The computed radiation patterns agree well with those obtained using CST. Gain and axial ratio as a function of frequency are shown in Fig. 10, where it can be seen that the spherical spiral provides a gain of 6.3 dB at 6 GHz and an axial ratio with a 3 dB bandwidth of 28% compared with a gain of 7 dB and an AR with a 3 dB bandwidth of 30% for an identical planar spiral.

The significance of the perfectly conducting sphere radius, r_2 , on the spiral's radiation characteristics has been investigated when $\epsilon_{r1} = 2$ and $h = 0.75$ cm at an operating frequency of 6 GHz. From Fig. 11 it can be seen that when $r_2 > 5$ cm the input impedance is approximately constant at $215 + j15 \Omega$ compared with $208 - j4 \Omega$ for a printed planar spiral. The variations of the gain and axial ratio with r_2 are shown in Fig. 12 where it can be seen that for larger r_2 the gain is 6.5 dB and the axial ratio is 2 dB.

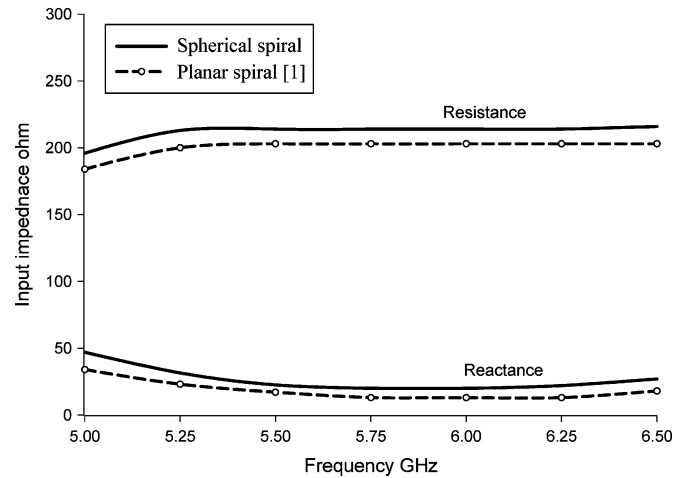


Fig. 13. Input impedance of a spiral above a large PEC sphere compared with that of an equivalent planar spiral.

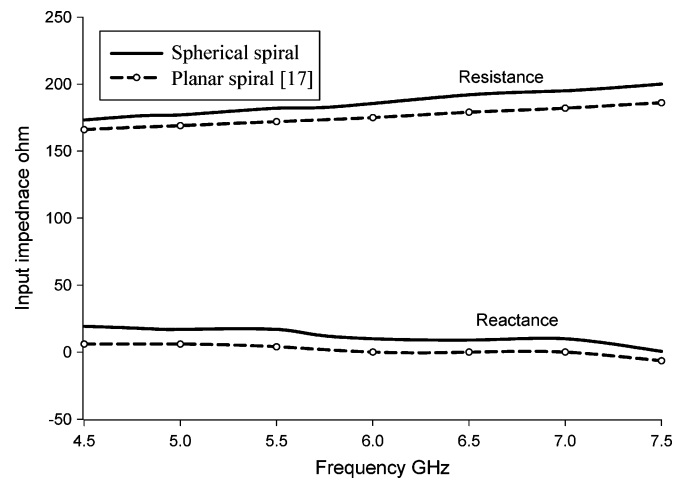


Fig. 14. Input impedance of a spiral printed on a 9 cm dielectric sphere compared with that of an identical planar spiral.

C. Large Sphere Considerations

As a further verification of the model, spirals above large spheres have been investigated. The input impedance of each spiral has been calculated and compared with that of an equivalent planar spiral.

A spherical spiral at a height of $h = 1.25$ cm above a perfectly conducting sphere has been modelled using the dimensions of a planar spiral given in [1]. The radius of the PEC sphere has been chosen as $r_2 = 7.75$ cm so that the overall sphere radius is $r_1 = 9$ cm. The computed input impedance agrees well with that of the planar spiral as shown in Fig. 13.

The input impedance of a spiral printed on a dielectric sphere has been calculated using the normalized planar spiral dimensions given in [17] at 6 GHz. In order to implement a valid comparison with the geometry of [17], the radius of the conducting spherical core has been reduced to $r_2 = 0$, that is, the problem is reduced to that of a spiral printed on a single layer dielectric sphere. The overall sphere radius has been chosen as $r_1 = h = 9$ cm. The calculated input impedance is shown in Fig. 14, where it can be seen that the impedance of a spherical

spiral approaches that of a planar spiral for a larger sphere radius.

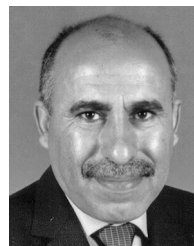
IV. CONCLUSION

The method of moments has been used to analyze an Archimedean spiral radiating in the presence of a layered sphere. The results have been validated against those obtained from CST for spirals above a perfectly conducting sphere and spirals printed on a grounded spherical substrate. The correctness of the model has been further verified by comparing the input impedance of a spiral above a large sphere with that of an equivalent planar spiral. Spirals conforming to a spherical surface have maintained the characteristics of a planar spiral such as circular polarization, gain and wide bandwidths. The addition of further dielectric layers can be implemented easily using the appropriate coefficients for the dyadic Green's function given in [13]. The presented model can be used to analyze other types of antennas that conform to a sphere by modifying the local co-ordinates α and β . Spherical arrays can also be modelled using the presented method since the model has been developed for antennas that are located arbitrarily on the spherical surface.

REFERENCES

- [1] H. Nakano, K. Nogami, S. Arai, H. Mimak, and J. Yamauchi, "A spiral antenna backed by a conducting plane reflector," *IEEE Trans. Antennas Propag.*, vol. 34, pp. 791–796, 1986.
- [2] H. Nakano, S. Okuzawa, K. Ohishi, H. Mimak, and J. Yamauchi, "A curl antenna," *IEEE Trans. Antennas Propag.*, vol. 41, pp. 1570–1575, 1993.
- [3] K. Hirose and H. Nakano, "An eccentric spiral antenna printed on a dielectric substrate," in *Proc. IEEE Antennas Propag. Soc. Int. Symp.*, 1995, vol. 1, pp. 190–193.
- [4] R. T. Gloutak and N. G. Alexopoulos, "Two arm eccentric spiral antenna," *IEEE Trans. Antennas Propag.*, vol. 45, pp. 723–730, 1997.
- [5] N. J. Champagne, J. T. Williams, and D. R. Wilton, "The use of curved segments for numerically modelling thin wire antennas and scatterers," *IEEE Trans. Antennas Propag.*, vol. 40, pp. 682–689, Jun. 1992.
- [6] S. K. Khamas and G. G. Cook, "Moment method analysis of printed wire spirals using curved piecewise sinusoidal subdomain basis and testing functions," *IEEE Trans. Antennas Propag.*, vol. 45, pp. 1016–1022, Jun. 1997.
- [7] H. Nakano, H. Yasui, and J. Yamauchi, "Numerical analysis of two arm spiral antennas printed on a finite size dielectric substrate," *IEEE Trans. Antennas Propag.*, vol. 50, pp. 362–369, 2002.

- [8] H. Nakano and K. Nakayama, "A curved spiral antenna above a conducting cylinder," *IEEE Trans. Antennas Propag.*, vol. 47, pp. 3–8, 1999.
- [9] K. Nakayama and H. Nakano, "Omnidirectional beam formation using spiral antennas above a conducting cylinder," *Electromagn.*, vol. 20, pp. 311–322, 2000.
- [10] A. Vallecchi and G. B. Gentili, "Broad band full scan coverage dual polarised spherical conformal phased array," *J. Electromagn. Waves Appl.*, vol. 16, pp. 385–410, 2002.
- [11] L. W. Li, C. P. Lim, and M. S. Leong, "Method of moments analysis of electrically large loop antennas: Nonuniform currents," *Proc. Inst. Elec. Eng. Microw. Antennas Propagat.*, vol. 146, pp. 416–420, 1999.
- [12] C. T. Tai, *Dyadic Green's Functions in Electromagnetics Theory*. Scranton, PA: Intext Educational, 1971.
- [13] L. W. Li, P. S. Kooi, M. S. Leong, and T. S. Yeo, "Electromagnetic dyadic Green's function in spherically multilayered media," *IEEE Trans. Microw. Theory Tech.*, vol. 42, pp. 2302–2310, 1994.
- [14] L. W. Li, M. S. Leong, P. S. Kooi, and T. S. Yeo, "Exact solutions of electromagnetic fields in both near and far zones radiated by thin circular-loop antennas: A general representation," *IEEE Trans. Antennas Propag.*, vol. 45, pp. 1741–1748, 1997.
- [15] N. Yuan, T. S. Yeo, X. C. Nie, L. W. Li, and Y. B. Gan, "Efficient analysis of electromagnetic scattering and radiation from patches on finite arbitrarily curved grounded substrates," *Radio Sci.*, vol. 39, 2004.
- [16] "CST Reference Manual," Computer Simulation Technology, 2006, Darmstadt, Germany.
- [17] H. Nakano, K. Hirose, I. Ohshima, and J. Yamauchi, "An integral equation and its application to spiral antennas on semi-infinite dielectric materials," *IEEE Trans. Antennas Propag.*, vol. 46, pp. 267–274, 1998.
- [18] J. S. R. Chisholm, *Vectors in Three Dimensional Space*. Cambridge, U.K.: Cambridge Univ., 1978.
- [19] S. Kirshnan, L. W. Li, and M. S. Leong, "Entire domain MoM analysis of an array of arbitrarily oriented circular loop antennas: A general formulation," *IEEE Trans. Antennas Propag.*, vol. 53, pp. 2961–2968, 2005.
- [20] L. W. Leung, K. M. Luk, K. Y. A. Lai, and D. Lin, "Theory and experiment of a coaxial probe fed hemispherical dielectric resonator antenna," *IEEE Trans. Antennas Propag.*, vol. 41, pp. 1390–1398, 1993.
- [21] R. F. Harrington, *Time Harmonic Electromagnetic Fields*. New York: Mc Graw-Hill, 1961.
- [22] Numerical Electromagnetics Code (NEC4WIN95VM) ver. 3.3, 2001.



Salam Khamas received the B.Sc. degree in electronic engineering from the University of Technology, Baghdad, Iraq, and the Ph.D. degree from the University of Sheffield, Sheffield, U.K., in 1985 and 1992, respectively.

From 1993 to 1998, he worked as a Research Associate in the Electronic and Electrical Engineering Department, Sheffield University. From 1998 to 2002, he was a Software Engineer at Alcatel Telecommunications and then at Nortel Networks. Since 2002, he has been a Lecturer in the Electronic and Electrical Engineering Department, University of Sheffield. His research interests include computational electromagnetics, conformal antennas, frequency independent antennas, array design and dielectric resonator antennas.